Spatial confinement and temporal dynamics of selectin ligands enable stable hematopoietic stem cell rolling

Bader Al Alwan[1‡], Karmen AbuZineh[1], Shuho Nozue[1], Aigerim Rakhmatulina[1], Mansour Aldehaiman[1], Asma S. Al-Amoodi[1], Maged F. Serag[1], Fajr A. Aleisa[1], Jasmeen S. Merzaban[1†] and Satoshi Habuchi[1†]**

[1] King Abdullah University of Science and Technology (KAUST), Biological and Environmental Science and Engineering Division, Thuwal 23955-6900, Saudi Arabia

*Correspondence should be addressed to S.H. (King Abdullah University of Science and Technology (KAUST), Biological and Environmental Sciences and Engineering Division, Thuwal 23955-6900, Saudi Arabia. E-mail: Satoshi.Habuchi@kaust.edu.sa, Tel.: +966-12-808-2483), or J.S.M. (King Abdullah University of Science and Technology (KAUST), Biological and Environmental Sciences and Engineering Division, Thuwal 23955-6900, Saudi Arabia. E-mail: Jasmeen.Merzaban@kaust.edu.sa, Tel.: +966-12-802-2383)

†These authors contributed equally to the work.

‡Current address: Stem cell and Regenerative medicine-King Abdullah International Medical Center (KAIMRC) – Kind Saud bin Abdulaziz University for Health Sciences.

Abstract

Hematopoietic stem/progenitor cell (HSPC) homing is initiated by tethering and rolling of the cells on endothelium through selectin-ligand interactions. Although multiple factors that affect the rolling behaviour of the cells have been identified, molecular mechanisms that enable slow and stable cell rolling remain elusive. Here, using a microfluidics-based single-molecule live cell fluorescence imaging, we reveal that unique spatiotemporal dynamics of selectin ligands on the membrane tethers and slings, which are distinct from that on the cell body, play an essential role in the rolling of the cell. Our results suggest that the spatial confinement of the selectin ligands to the tethers and slings together with the rapid scanning of a large area by the selectin ligands increases the efficiency of selectin-ligand interactions during cell rolling, resulting in slow and stable rolling of the cell on the selectins. Our findings provide novel insights and contribute significantly to the molecular-level understanding of the initial and essential step of the homing.

Introduction

Delivering circulatory cells to specific sites in the body is central to many physiological functions, from immunity to cancer metastasis, which is achieved by their interactions with the surface of endothelium under the presence of external shear forces.(Ley et al., 2018; Quail & Joyce, 2013) These cellular interactions are controlled by a number of adhesion molecules that include selectins and integrins and their corresponding ligands.(Kolaczkowska & Kubes, 2013) So far, molecular mechanisms of cell adhesion have been investigated by characterizing migration behaviour at the cellular level in the presence of shear force exerted to the migrating cells and/or characterizing binding behaviour of the adhesion molecules with their ligands at the molecular level by applying external force to the bonds using, for example, single-molecule force spectroscopy technique.(Alon, Hammer, & Springer, 1995; Marshall et al., 2003; McEver & Zhu, 2010) However, under physiological flow conditions, interactions between adhesion molecules and their ligands occur under a spatiotemporal rather heterogeneous cellular environment. Thus, without capturing real-time nanoscopic spatiotemporal interactions of adhesion molecules and their ligands at the molecular level in the cellular environment, one cannot develop a complete picture of complicated cellular interactions that exist.

Hematopoietic stem/progenitor cell (HSPC) homing is an important biological phenomenon in which transplanted HSPCs travel from peripheral blood to the bone marrow.(Magnon & Frenette, 2008) The homing of HSPCs to bone marrow is a multistep process that is initiated by tethering and rolling of the cells on endothelium (Ley, Laudanna, Cybulsky, & Nourshargh, 2007; Magnon & Frenette, 2008; McEver & Zhu, 2010; Sundd, Pospieszalska, & Ley, 2013). The initial step of homing is mediated by the binding of homing receptors expressed on endothelial cells, E- and P-selectin (Lehr & Pienta, 1998; Schweitzer et al., 1996), to their

ligands expressed on the HSPCs that include CD44 (Dimitroff, Lee, Rafii, Fuhlbrigge, & Sackstein, 2001; Ponta, Sherman, & Herrlich, 2003) and PSGL-1 (Goetz et al., 1997; Yago et al., 2010). HSPCs are tethered to the endothelium by the selectin-ligand interactions resulting in their rolling along the endothelium at shear stress of several dynes cm^{-2} generated by the blood flow (Frenette, Subbarao, Mazo, von Andrian, & Wagner, 1998; Hidalgo, Weiss, & Frenette, 2002; Mazo et al., 1998). Although multiple factors that affect the rolling behaviour of the cells have been identified, including spatial clustering of the ligands (Abbal et al., 2006), formation of membrane tethers and slings (Sundd et al., 2012), and shear force-dependent selectin-ligand interactions (Marshall et al., 2003), spatiotemporal dynamics of selectin ligands during this initial step of homing and its contribution to slow and stable cell rolling are not well understood. This is due the lack of an experimental method that enables capturing real-time nanoscopic spatiotemporal interactions of adhesion molecule and their ligands at the molecular level in the cellular environment.

In this study, using a microfluidics-based single-molecule live cell fluorescence imaging technique, we showed that the unique spatiotemporal dynamics of selectin ligands on the membrane tethers and slings play an essential role in the rolling of the cell. We demonstrated that the membrane tethers are formed from single microvilli on the cells and this provides a mechanism to spatially localise selectin ligands, in particular PSGL-1 and CD44, on these tethers and slings. Furthermore, this work also established that due to the detachment of the cell from the actin cytoskeleton during the formation of the tethers, fast and random diffusional motion of selectin ligands is exhibited along these structures (i.e., tethers and slings) in contrast to the slow and confined motion of the ligands on the cell body. Our results suggest that the spatial confinement of the selectin ligands to the tethers and slings together with the rapid scanning of a

large area by the selectin ligands increases the efficiency of selectin-ligand interactions during cell rolling, resulting in slow and stable rolling of the cell on the selectins.

Results and Discussion

We developed a microfluidics-based single-molecule fluorescence imaging platform to capture and characterize molecular level spatiotemporal dynamics of selectin ligands that occur during cell rolling on selectins (AbuZineh et al., 2018). To this end, we deposited recombinant human (rh) E-selectin on the surface of a microfluidic chamber (Supplementary Fig. 1) and injected a suspension of KG1a cells, a human leukemic progenitor cell line often used as a model system of HSPCs (AbuSamra et al., 2015; AbuSamra et al., 2017; Merzaban et al., 2011), into the fluidic chamber at the shear stresses of 1 – 8 dyne cm^{-2} using a syringe pump (Fig. 1a, Supplementary Fig. 2, Supplementary Table 1). CD44 and PSGL-1, two selectin ligands expressed on KG1a cells and $CD34^{pos}$-HSPCs, were immunolabelled by fluorophore (either Alexa-Fluor-488, Alexa-Fluor-555, or Alexa-Fluor-647)-conjugated antibodies (515 mAB and KPL-1 mAB for CD44 and PSGL-1, respectively) and introduced into the chamber. Fluorescence-activated cell sorting (Supplementary Fig. 3, 4) and fluorescence imaging of labelled cells (Supplementary Fig. 5, Supplementary Note 1) was used to confirm the binding specificity of these antibodies. The cytoplasmic membrane of the KG1a cells was fluorescently-stained using Vybrant DiO dye.

Epi-fluorescence images of the Vybrant DiO-stained KG1a cells rolling on E-selectin at a shear stress of 2 dyne cm^{-2} illustrated the formation of membrane tethers and slings (Supplementary Fig. 6) (Sundd et al., 2012). Membrane tethers that appear during cell rolling on selectins are believed to play a critical role in the stable rolling of the cells. Previous studies demonstrated that live cells roll on a selectin surface more stably compared to fixed cells or to microspheres coated

with selectin ligands (Sundd et al., 2013). These observations suggest that tethers help decrease the tension exerted on selectin-ligand bonds and thereby reduce the probability of breaking these interactions. This stronger binding is consistent with previous studies from our lab illustrating that the off rate of binding between selectin ligands and E-selectin is low (AbuSamra et al., 2015; AbuSamra et al., 2017).

Two-color epi-fluorescence imaging of the cell membrane and CD44 of the KG1a cells showed perfect colocalisation of the two images, demonstrating that the tethers and slings are fully covered by CD44 molecules (Fig. 1b, c, Supplementary Note 2). The tethers and slings were formed at all the shear stresses used in this study (1 – 8 dyne cm^{-2}, Supplementary Fig. 7, Supplementary Movie 1). The formation of tethers and slings was also observed for primary human $CD34^{pos}$-HSPCs at a shear stress of 2 dyne cm^{-2} (Supplementary Fig. 8). These are in contrast to the previous study on neutrophils rolling over P-selectin, which showed the formation of the tethers and slings only at shear stresses higher than 6 dyne cm^{-2} (Supplementary Note 3) (Sundd et al., 2012). The length of the tethers and slings range in size between several micrometres to tens of micrometres (Supplementary Fig. 9, 10). Interestingly, on occasion, tethers and slings longer than 100 micrometres were observed (Supplementary Fig. 9). Time-lapse fluorescence images of CD44 clearly demonstrated that a tether detached from the E-selectin surface is converted into a sling within several hundreds of milliseconds in both KG1a cells and primary human $CD34^{pos}$-HSPCs (Supplementary Fig. 11, 12 Supplementary Movie 2, Supplementary Note 4) (Marki, Gutierrez, Mikulski, Groisman, & Ley, 2016). Given that the primary human $CD34^{pos}$-HSPCs showed very similar structures to our model $CD34^{pos}$ cell line and that access to these primary cells is limited, we chose to focus on KG1a cells for all subsequent experiments.

While the slings are persistent structures, we also observed a retraction of the slings during cell rolling (Supplementary Fig. 13, Supplementary Movie 3). In contrast to the contiguous distribution of CD44 on the tethers and slings (Fig. 1d), we found that PSGL-1 shows a discrete spatial distribution on the tethers and slings (Fig. 1e, Supplementary Movie 4, 5). The PSGL-1 molecules on the tethers and slings displayed perfect spatial overlap with the cell membrane and CD44 (Fig. 1f, Supplementary Fig. 14, 15).

By reconstructing 3D fluorescence images of CD44 (Fig. 1g, h, Supplementary Fig. 16) and PSGL-1 (Supplementary Fig. 17), a clear and obvious formation of the tethers and slings during cell rolling along with the spatial distributions of the selectin ligands on the tethers and slings was possible. The side views of the 3D images visibly show the formation of multiple tethers and slings during cell rolling over E-selectin (Fig. 1g, h, Supplementary Fig. 16, Supplementary Note 5). These images also unambiguously demonstrated that the tethers and slings are entirely covered with the CD44 and PSGL-1 molecules in a distinct spatial distribution (i.e. contiguous and discrete distributions for CD44 and PSGL-1, respectively). In addition, the time-lapse 3D images captured the elongation of tethers (Supplementary Fig. 18) and change in the Z-axis position of the slings (Supplementary Fig. 19) during cell rolling. The entire tethers were consistently covered by the selectin ligands during their elongation. We also often observed the formation of anchoring points on the tethers (Fig. 1d, Supplementary Fig. 20).

The fluorescence images of CD44 and PSGL-1 on the tethers and slings sometimes show bright spots at their tips (Fig. 1h and 2a, Supplementary Fig. 21), indicating clustering of the selectin ligands at the tethering points. The clustering of selectin ligands at the tethering points was further investigated by calculating the number of PSGL-1 molecules at each spot on the tethers and slings. Our calculation demonstrated that each PSGL-1 spot distributed on the tethers and

slings mainly corresponds to a single PSGL-1 molecule (Fig. 2b). The distributions were fitted to Poisson distribution, suggesting that the number of PSGL-1 molecules at each spot is determined stochastically (i.e. absence of a mechanism that colocalislocalies the PSGL-1 molecules together, Supplementary Note 6). On the other hand, we found that multiple PSGL-1 molecules are present at the tethering point (4.1 molecules, Fig. 2c) and anchoring point (2.3 molecules, Fig. 2d), suggesting the spatial clustering of the selectin ligands at the tethering and anchoring points. The significant deviation from Poisson distribution observed for the tethering and anchoring points (Fig. 2c, d) indicates the presence of a specific mechanism that supports the spatial clustering of PSGL-1 at these points, which facilitates the formation of the tethering and anchoring points (Supplementary Note 6). Data from our lab has shown that the binding of E-selectin to its ligands is limited by a slow-on rate (AbuSamra et al., 2015; AbuSamra et al., 2017) and this observation that clustering of the ligands (i.e. CD44 and PSGL-1) occurs at anchor points helps to explain how the cell in flow can overcome this "slow on" rate and enhance the binding of E-selectin to its ligands ultimately through the increase in the local concentration of the ligands.

To investigate the effect of the clustering of the selectin ligands on the formation of tethers/slings and on the rolling behaviour of the cell, we disrupted the clusters of CD44 by treating the cells with methyl-β-cyclodextrin (MβCD) (Abbal et al., 2006; AbuZineh et al., 2018; Setiadi & McEver, 2008). Cholesterol existing in the cell membrane is extracted by this treatment, leading to the disruption of lipid rafts domains. Super-resolution fluorescence images of CD44 on the KG1a cells clearly showed that the 200 nm-size CD44 clusters existing on the control cells are disrupted by the MβCD treatment (Fig. 2e, f) (AbuZineh et al., 2018). Scanning electron microscopy (SEM) images of the control and MβCD-treated KG1a cells clearly revealed that

microvilli existing on the control cells (Fig. 2g, Supplementary Fig. 22a) disappear upon the MβCD treatment (Fig. 2h, Supplementary Fig. 22b). These results are reminiscent of previous data from our lab showing that CD34 plays a key role in the formation of microvilli structures since once they are knocked down, microvilli structures disappear (AbuSamra et al., 2017). This result strongly suggests that the CD44 molecules localise on the microvilli in the control cells. We found that the formation of the tethers and slings is extremely inefficient under the MβCD-treated condition (Fig. 2i, Supplementary Note 7) as well as when CD34 is knocked down (Fig. 2j, Supplementary Fig. 23, 24). While the tethers and slings are formed in more than 90 % of the control cells rolling over E-selectin (Supplementary Movie 6), they are observed in less than 10 % of the MβCD-treated cells and CD34 knockdown cells. Further, the length of the tethers and slings formed during the rolling of the MβCD-treated cells were much shorter than those formed in the control cells (Fig. 2k). The fluorescence images of CD44 on the MβCD-treated cells and CD34 knockdown cells never showed bright spots (i.e. clusters of CD44) at the tethering points (Fig. 2i and 2j). These results demonstrate that the clustering of the selectin ligands contributes to both initial binding to the surface E-selectin (i.e. tether formation) as well as the elongation of the tethers against the tension exerted to the tethering point during cell rolling. Since CD34 knockdown KG1a cells (AbuSamra et al., 2017) and MβCD-treated KG1a cells (AbuZineh et al., 2018) exhibit approximately 3-5 times faster rolling velocity compared with control cells and showed more unstable rolling (i.e. faster detachment) on E-selectin, our findings suggest that the efficient formation of the tethers and slings and their strong resistance to shear stress due to the spatial clustering of the selectin ligands on the microvilli enables the slow and stable rolling of the cells (Supplementary Note 8). Our finding also suggests that the

microvilli play a key role in the spatial clustering of the selectin ligands and the formation of the tethers and slings during cell rolling over E-selectin.

Based on these findings, we next sought to investigate the mechanism of the formation of the tethers. To that end, we calculated the total number of the PSGL-1 molecules on a single tether during its elongation (Fig. 3a). The time lapse images of PSGL-1 showed that the total number of the PSGL-1 molecules on the tether estimated by the integrated fluorescence intensity of PSGL-1 over the entire tether is almost constant during the tether elongated from 75 μm to 110 μm (Fig. 3b, c, d). We also calculated the total number of the PSGL-1 molecules on single tethers and slings at different shear stresses (Fig. 3e) using the lengths of the tethers/slings (Fig. 3f, Supplementary Fig. 9) and the distances between the adjacent PSGL-1 molecules on the tethers/slings at different shear stresses (Fig. 3g, Supplementary Fig. 25). The calculation showed that the total number of the PSGL-1 molecules on single tethers and slings is almost constant over the 1 – 8 dyne cm^{-2} although the tethers and slings were two times longer at 8 dyne cm^{-2} compared with those at 1 dyne cm^{-2} (Fig. 3e). Given the localisation of PSGL-1 and CD44 on the microvilli (Abbal et al., 2006; AbuZineh et al., 2018; Miner et al., 2008; Moore et al., 1995), our results strongly suggest that single tethers and therefore slings are formed from single microvilli upon their binding to the surface E-selectin (Fig. 3h). This is supported by our observation that the tethers and slings are always covered entirely by CD44 and PSGL-1 (Fig. 1b, f). If the tethers are formed from multiple microvilli, this would result in discrete patches of CD44 and PSGL-1 clusters on the tethers and slings.

Previous studies suggested that the localisation of selectin ligands to microvilli enables them to interact with selectins during the initial step of homing (Miner et al., 2008; Moore et al., 1995). Our findings here extend this to the tethers and slings. During cell rolling, CD44 and PSGL-1 are

spatially redistributed to the entire tethers and slings by the conversion of single microvilli to the tethers. This redistribution significantly increases the exposure of these selectin ligands to the surface E-selectin, promoting clustering and efficient selectin-ligand binding that leads to mechanisms that help overcome the slow-on rate (AbuSamra et al., 2015; AbuSamra et al., 2017) leading to slow and stable rolling.

Single-molecule imaging revealed that the PSGL-1 molecules show diffusional motion on the tethers and slings (Fig. 4a, Supplementary Movie 4, 5). We analyzed their motion using mean square displacement (MSD) analysis of the single-molecule diffusion trajectories (Supplementary Fig. 26, Supplementary Note 9). The MSD analysis showed that the PSGL-1 molecules on the tethers and slings have a mean diffusion coefficient of approximately 0.2 $\mu m^2 s^{-1}$ (Fig. 4b, Supplementary Fig. 27), which is much faster than those reported for membrane proteins including PSGL-1 on neutrophils (0.003 $\mu m^2 s^{-1}$) (Gaborski, Clark, Waugh, & McGrath, 2008). The MSD analysis also demonstrated that the PSGL-1 molecules display random diffusion on the tethers and slings (i.e. linear relationship between the MSD and time lag, Fig. 4c). We conducted single-molecule tracking experiments of the PSGL-1 molecules on the control cells (i.e. localised on microvilli) (Fig. 4d). The MSD analysis of the diffusion trajectories showed that the PSGL-1 molecules on the control cells diffuse much slower than those distributing on the tethers and slings (i.e. mean diffusion coefficient of 0.1 $\mu m^2 s^{-1}$, Fig. 4e, Supplementary Note 10). The analysis also revealed that the PSGL-1 molecules on the control cells show a confined diffusion with a confinement area of 0.29 μm^2 (Fig. 4c, f, Supplementary Fig. 28, Supplementary Note 10). Due to the distinct rates and modes of the diffusion, the PSGL-1 molecules on the tethers and slings cover much larger displacement areas compared with those restricted to the microvilli (0.14 μm^2 and 0.26 μm^2 for tethers and slings, respectively compared

with 0.038 μm^2 for microvilli) during the several hundreds of milliseconds of the lifetime of the tethers (Chen & Springer, 1999; Schmidtke & Diamond, 2000). The difference becomes even larger when more stable structures (i.e. tethers with multiple anchoring points and non-retracting slings that exist for more than several seconds) are formed during cell rolling.

The larger motional freedom (i.e. faster and random diffusion) of the PSGL-1 molecule on the tethers and slings compared with those localised to the microvilli and the merger of multiple tethers into a single tether (i.e. occurring during cell rolling; Fig. 4g, Supplementary Movie 7) imply the involvement of the actin cytoskeleton. We thus conducted a two-color fluorescence imaging experiment of CD44 (labelled by either Alxa-Fluor-488- or Alxa-Fluor-647-conjugated antibodies) and actin (labelled by either silicon-rhodamine-conjugated jasplakinolide (Lukinavicius et al., 2014) or Alexa-Fluor-488-conjugated phalloidin). The fluorescence image of CD44 and actin on the control KG1a cells showed perfect colocalisation (Fig. 4h). On the other hand, we did not observe any fluorescence signal of actin from the tethers and slings in most cells rolling over E-selectin. In some rare cases, we found that actin exists along the tethers and slings of the rolling cells, but in a form of small fragmented patches (Fig. 4i). This result unambiguously demonstrates that the cell membrane is detached from the cortical actin cytoskeleton during the formation of the tethers, consistent with previous force spectroscopy studies that indicated the detachment (Evans, Heinrich, Leung, & Kinoshita, 2005; Heinrich, Leung, & Evans, 2005; Shao, Ting-Beall, & Hochmuth, 1998). Since PSGL-1 and CD44 on the control cells are directly or indirectly anchored to the actin cytoskeleton in the microvilli by actin binding ERM proteins (Moore et al., 1995; Snapp, Heitzig, & Kansas, 2002; Wang et al., 2014), the formation of the tethers and therefore the detachment of the membrane from the actin

cytoskeleton would cause a significant enhancement in the motional freedom of PSGL-1 and CD44, consistent with the results obtained from the single-molecule tracking analysis.

To form a selectin-ligand bond, the ligand molecules on the rolling cell have to be located within tens of nanometres distance from the surface E-selectin molecules (Cummings & McEver, 2009). If the locations of the PSGL-1 molecules are fixed, the probability to find the surface E-selectin molecules within this distance is relatively low. Thus, the fast and random motion of the selectin ligands on the tethers and slings, which enables them to scan large surface area during a limited lifetime of tethers (with anchoring points) and slings, should facilitate efficient binding of the selectin ligands to the surface E-selectin and thus enable slow and stable rolling of the cell (Fig. 4j).

In conclusion, our results suggest that during the initial step of HSPC migration, the selectin ligands are spatially confined to the tethers and slings through the development of the tethers from single microvilli and their motional freedom on the tethers and slings is enhanced by the detachment of the membrane from actin cytoskeleton during the formation of the tethers. These mechanisms enable the efficient utilization of the limited amount of the selectin ligands, which contributes to overcome the slow on rate of binding to the underlying E-selectin (AbuSamra et al., 2015; AbuSamra et al., 2017) to achieve effective selectin-ligand binding, resulting in this slow and stable cell rolling.

Materials and Methods

Cell culturing and treatments. Human acute myelogenous leukemia cell lines, KG1a cells (ATCC CCL-246.1) were maintained in the lab using cell culturing facility in RPMI 1640 (1×) media (Gibco) that contains 10 % fetal bovine serum (Corning) and antimicrobial agents (100 U

ml^{-1} penicillin, 100 µg ml^{-1} streptomycin, Hyclone) incubated at 37° C in presence of controlled 5% CO_2. For the disruption of lipid raft microdomains, the KG1a cells were treated with methyl-β-cyclodextrin (MβCD). Briefly, 10^6 ml^{-1} KG1a cells were washed three times by HBSS buffer (pH = 7.0 – 7.4) and incubated in serum-free Iscove's modified Dulbecco's medium (IMDM, Gibco) with 10 mM HEPES buffer (Sigma) and 10 mM MβCD (Sigma) at 37° C for 30 min. The viability of the cells after the treatment was confirmed by trypan blue staining. For siRNA knockdown of CD34 in KG1a cells, KG1a cells were first collected and treated for 20 min at 37°C with bromelain (250 ug/ml; Sigma) in RPMI media with 10% FBS. Cells were then washed twice with PBS and prepared for transfection. The bromelain treated KG1a cells were then transfected using 250 pmol of CD34 siRNA (Silencer Select, Life technologies; 4392420-s2644) or 250 pmol of a scrambled control siRNA (Silencer Select, Life technologies; 4390843). Transfection was done using the SE Cell Line 4D-Nucleofector™ X Kit (Lonza). The company protocol was followed to achieve the knockdown. Cells were then collected after 48 h and prepared for Western blot analysis to determine the extent of the CD34 inhibition.

Preparation of human $CD34^{pos}$ HSPCs. Primary human $CD34^{pos}$ HSPCs isolated from umbilical cord blood ($CD34^{pos}$HSPCs) and the mononuclear cells (MNC) from whole cord blood were purchased from ALL Cells (USA). For $CD34^{pos}$HSPCs isolation from whole cord blood, the MNCs were washed and filtered through a 100 µm cell strainer (BD Falcon) followed by lineage depleton by negative selection using a lineage cell depletion cocktail (Milteny Biotec). The lineage depleted fraction was stained with 13 markers for lineage-specfic monoclonal antibodies FITC (CD2, CD3, CD4, CD11b, CD14, CD15, CD24, CD10, CD41, CD20, CD66c, CD127, CD33) (Biolegend and BD) and Pacific blue conjugated anti-CD34 (Biolegend), for 30 min at 4°C. Before sorting, 7-AAD was added to the tubes. Afterwards, 13Lin−$CD34^{pos}$ cells

were collected by the fuorescence- activated cell sorter (FACSAria, BD Biosciences, San Jose, CA, USA).

For $CD34^{pos}$ HSPCs, the cells were thawed using stem span SFEM II medium (Stem Cell Technologies, Canada) and washed 1x with the same medium. The cells were resuspended in 1 mL of medium contained 1x Stem Span Cytokine Cocktail CC100 (Stem Cell Technologies, Canada) in 24-well plate, then the cells were analyzed within 24 hours.

Preparation and functionalization of the microfluidic chambers. Commercially available microfluidic chambers, µ-slide VI 0.1 uncoated (ibidi GmbH) were used for *in vitro* cell rolling assay. Recombinant homodimeric human (rh) E-selectins (Sino Biological) were deposited on the inner surface of the microfluidic chambers by incubating with 20 µl of the rh E-selectin (0.5 – 4 µg ml^{-1}) at 4° C for overnight. After the incubation, the chambers were washed 3 times using 1× Hank's balanced Salt Solution (HBSS, Gibco) and blocked with 1% Bovine Serum Albumin (BSA, Sigma Aldrich) by incubating the chambers at 4° C for 1-2 hours. The chambers were then washed by 1× HBSS three times.

Estimation of the surface density of the rh E-selectin. A monoclonal anti-human E-selectin antibody (HCD62E clone, Biolegend) was labelled with Alexa-Fluor-647 dye as described below. The Alexa-Fluor-647-conjugated anti-E-selectin was diluted into HBSS at the concentration of 10 µg ml^{-1}. 20 µl of the Alexa-Fluor-647-conjugated anti-E-Selectin antibody was introduced into the microfluidic chambers on which the homodimeric rh E-Selectin was deposited. The chambers were incubated with the antibody at 4° C for 1 hour. The fluorescence from the Alexa-Fluor-647-conjugated anti- E-Selectin antibody bound to the surface rh E-selectin was recorded using a custom-built single-molecule fluorescence imaging setup (see below). The surface density of the rh E-selectin was calculated by comparing the integrated

fluorescence intensity obtained from a unit area (1 μm^2) of the rh E-selectin-deposited surface with the intensity obtained from single rh E-Selectin molecules labelled by the Alexa-Fluor-647-conjugated anti-E-Selectin antibody. The fluorescence intensity from single rh E-Selectin molecules labelled by the antibodies was determined by depositing the Alexa-Fluor-647-conjugated anti-E-Selectin antibody on the rh E-selectin-deposited surface at very low concentration (0.02 $\mu g\ ml^{-1}$) and measuring the fluorescence intensities of the individual fluorescent spots obtained from the single rh E-selectin molecules labelled by the antibodies.

Cell rolling assay using bright-filed microscope. The rh E-selectin-deposited microfluidic chambers were connected to a syringe pump (Harvard Apparatus, PHD Ultra) using a silicone tubing (inner diameter of 0.8 mm, ibidi GmbH) and mounted on an inverted optical microscope (Olympus, CKX41). KG1a cells were suspended in HBSS buffer containing 0.7 mM of Ca^{2+} (anhydrous $CaCl_2$, Sigma Aldrich) and 1 % (w/v) BSA. The rolling behaviour of the cells in this perfusion buffer was observed using the inverted light microscope that is equipped with a 20× objective lens (Olympus, LCAch N 20X PHP) and XC10 CCD camera (Olympus). The transmitted images were recorded by the CCD camera using CellSens imaging software provided by Olympus. All images were recorded at the frame rate of 15 fps with 30 ms exposure time. The pixel size of the CCD camera is 6.45 µm. The KG1a cells were perfused into the microfluidic chamber mounted on the microscope stage at the flow rate of 100 dyne cm^{-2}, then the flow rate was decreased gradually to reach a constant shear stress of 4 dyne cm^{-2}, 2 dyne cm^{-2}, 1 dyne cm^{-2}, 0.5 dyne cm^{-2}, or 0.25 dyne cm^{-2} where cell rolling behaviour was monitored for 78 seconds in each experiment. The rolling velocities were calculated using CellSens or TrackMate, an Image J plugin. The rolling velocities were estimated by measuring the distance travelled by each cell after being bound to the immobilized rh E-selectins. The number of the bound cells was

determined by counting the number of the attached cells in a field of view (0.444 mm × 0.335 mm size).

Fluorescence labelling of the antibodies. The fluorescence labelling of the antibodies by Alexa-Fluor-488 dye (Invitrogen), Alexa-Fluor-555 dye (Invitrogen), and Alexa-Fluor-647 dye (Invitrogen) was conducted by following the manufacturer's instructions. The labelled antibodies were mouse anti-human E-selectin (HCD62E clone), mouse anti-human CD44 (515 clone, Ms IgG1, κ, BD Bioscience) and mouse anti-human PSGL-1 (KPL-1 clone, Ms IgG1, κ, BD Bioscience) and mouse anti-human CD34 (QBEND 10 clone, Ms IgG1, Bio-Rad). Briefly, the Alexa-Fluor dyes conjugated to N-hydroxysuccinimide (NHS) were dissolved in dimethylsulfoxide (DMSO, Sigma-Aldrich, 276855) to a final concentration of 10 mg ml^{-1}. The antibodies were dissolved in 0.1 M sodium bicarbonate (pH = 8.3 – 8.4) at a concentration of 6.5 mg ml^{-1}. 30.7 µl of the antibody solution and 2 µl Alexa-Fluor dye solution (i.e. mixing ratio of ten to one, which corresponds to the dye to antibody molar ratio of approximately 120 to 1) were mixed and incubated for 1 hour at room temperature. After the labelling reaction, 467 µl of HBSS was added to the reaction mixture. Free dyes in the mixture were removed by using a spin filter (Pall Corporation, Nanosep centrifugal devices with Omega membrane, OD010C34) at a centrifuge speed of 10,000 xg for 5 min. The solution was resuspended in HBSS and the centrifugation was repeated several times. The final concentration of the antibodies and the labelling degree were determined by UV-vis absorption spectra of the Alexa-Fluor dye-conjugated antibodies. The degree of labelling was in the range of 4 – 9 dyes per antibody.

Fragmentation and fluorescence labelling of the antibodies. For the digestion and purification of the anti-PSGL-1 antibody (KPL-1 clone, IgG1), we used Pierce Mouse IgG1 Fab and F(ab´)2 Preparation Kit or Pierce Mouse IgG1 Fab and F(ab´)2 Micro Preparation Kit (Thermo Scientific).

The kit uses immobilized ficin protease to efficiently digest mouse IgG1 into Fab or F(ab')2 fragments, depending on the concentration of cysteine and solution pH. Briefly, the digestion buffer was prepared by dissolving 43.9 mg of cysteine•HCl in 10 ml of the supplied Mouse IgG1 digestion buffer (pH = 5.6) to produce Fab fragments. Then, the immobilized enzyme was dispensed into the spin column, centrifuged and washed using the prepared digestion buffer. The antibody (1 mg ml^{-1}, 125 µl) was desalted using the accompanied Zeba column. The flow through of at least 100 µl that contained the antibody was incubated with the immobilized enzyme for 3-5 hours at 37 °C on an end-over-end mixer, which digested the antibody into Fab fragments. After the incubation, the column was put into a 2 ml collection tube and centrifuged at 5000 × g for 1 min to collect the digested antibodies. The collected flow through was incubated with protein A column for 10 min at room temperature on an end-over-end mixer, followed by centrifugation at 1000 × g for 1 min to separate the Fab fragments from Fc and undigested antibodies. The flow through that contained Fab fragments was collected. After the fragmentation and purification, concentrations of the anti-PSGL-1 antibody (KPL-1 clone, IgG1) and its fragments were determined by measuring the absorbance at 280 nm using UV-vis spectrophotometer (Thermo Scientific, NanoDrop 2000).

Fluorescence labelling of the Fab fragment of the anti-PSGL-1 antibody by the Alexa-Fluor dyes conjugated to N-hydroxysuccinimide (NHS) was conducted in a manner similar to the labelling of the whole antibody. The Fab fragment and the dye were mixed at the mixing ratio of thirty to one, which corresponds to the dye to antibody molar ratio of approximately 120 to 1. The degree of labelling with this mixing ratio was in the range of 1 – 3 dyes per Fab fragment.

Fluorescence labelling of the primary cells and KG1a cells. Prior to immunostaining of the KG1a and primary cells, the cells were incubated with Fc blocker (0.15 – 0.3 ml for each 1 x 10^6

cells, Innovex biosciences) on ice for 45 minutes, then washed three times with 1x HBSS. The cells were immunostained by either Alexa-Fluor-488-conjugated anti-PSGL-1, Alexa-Fluor-555-conjugated anti-PSGL-1, Alexa-Fluor-647-conjugated anti-PSGL-1, Alexa-Fluor-488-conjugated anti-CD44, or Alexa-Fluor-647-conjugated anti-CD44 for 45 min on ice at a concentration of 5 μg for each 10^6 cells. The immunostained cells were suspended in a Fluorobrite (Gibco) perfusion buffer containing 0.7 mM of Ca^{2+} at the density of $0.5 – 1 \times 10^6$ cells ml^{-1}. Then, the cells were injected into the rh E-selectin-deposited microfluidic chambers using the silicone tubing connected to the syringe pump. The KG1a or primary cells were perfused into the microfluidic chamber mounted on the stage of an inverted fluorescence microscope (Olympus, IX71) at the flow rate of 100 dyne cm^{-2}. Then the flow rate was decreased gradually to reach a constant shear stress of 1 – 8 dyne cm^{-2} where real-time fluorescence images of CD44 or PSGL-1 on the live KG1a or primary cells were recorded by using EMCCD camera connected to the iQ3 software (see below).

Two-color fluorescence imaging of CD44 and PSGL-1 on the KG1a cells were conducted by immunostaining both CD44 and PSGL-1 with a combination of either Alexa-Fluor-488-conjugated anti-CD44 and Alexa-Fluor-647-conjugated anti PSGL-1 or Alexa-Fluor-647-conjugated anti-CD44 and Alexa-Fluor-488-conjugated anti PSGL-1. For the two color immunostaining, the KG1a cells were incubated simultaneously with the two antibodies (5 μg of each antibody for 10^6 cells) on ice for 45 min.

Two-color fluorescence imaging of CD44 and CD34 on KG1a and CD34 knockdown cells were conducted by immunostaining both CD44 and CD34 with a combination of Alexa-Fluor-647-conjugated anti CD44 and Alexa-Fluor-488-conjugated anti-CD34. For the two color immunostaining, KG1a cells were first incubated with CD44 antibody and then with CD34

antibody (5 µg of each antibody for 10^6 cells). Each incubation was done on ice cooled condition for 45 min.

We used Vybrant DiO (Molecular Probe) for staining plasma membrane of KG1a cells. The harvested and counted KG-1a cells were washed three times with serum free 1x IMDM. The staining solution was prepared by adding 1 µl of the Vybrant DiO stain to each 1 ml serum free IMDM. The 10^6 cells after washing were suspended in the 1 ml staining solution, mixed and incubated at 37° C for 15 min. The stained cells were washed twice in 1x serum free IMDM and once with 1x HBSS and resuspendend in the Fluorobrite perfusion buffer containing 0.7 mM of Ca^{2+} at the density of $0.5 – 1 \times 10^6$ cells ml^{-1}. For the two-colour fluorescence imaging of the cell membrane and the selectin ligands (either CD44 or PSGL-1), the Vybrant DiO-stained KG1a cells were incubated with the Alexa-Fluor-647-conjugated anti-CD44 or anti-PSGL-1 antibodies (5 µg for each 10^6 cells) on ice for 45 min.

We used silicon rhodamine (SiR)-conjugated jasplakinolide (Cytoskeleton, Inc.) for staining actin cytoskeleton of the live KG1a cells. The harvested KG1a cells were washed three times with 1x HBSS. The staining solution was prepared by adding 1 µl of DMSO contining1 mM of SiR-jasplakinolide and 1 µl of DMSO containing 10 mM of verapamil into 998 µl Dulbecco's modified Eagle medium (DMEM) containing 10 % bovine serum. The 10^6 cells after washing were suspended in the 1 ml staining solution, mixed and incubated at 37° C for 1 hour in presence of 5% CO_2. The stained cells were washed three times using 1x HBSS and resuspended in the Fluorobrite perfusion buffer containing 0.7 mM of Ca^{2+} at the density of $0.5 – 1 \times 10^6$ cells ml^{-1}. For the two-colour fluorescence imaging of the actin cytoskeleton and cell membrane, the SiR-stained (i.e. actin-labelled) KG1a cells were incubated with Vybrant DiO stain at 37 °C for 15 min.

The fluorescence imaging experiment of CD44 and cell membrane on the MβCD-treated live KG1a cells was conducted in a way similar to that on the control KG1a cells by using Vybrant DiO for the membrane stain and Alexa-Fluor-647-conjugated anti-CD44 for the immunostaining of CD44. The fluorescence labelling was conducted immediately after treating the cells with MβCD.

We used Alexa-Fluor-488-conjugated phalloidin (molecular Probes-Thermo Fisher Scientific) and anti-CD44 for staining actin cytoskeleton and CD44 of the fixed KG1a cells. The harvested KG1a cells were fixed in 3 % (w/v) paraformaldehyde (Electron Microscopy Sciences) and 0.2 % (w/v) glutaraldehyde (Electron Microscopy Sciences) in HBSS for 20 min at room temperature. The fixed cells were blocked with 10 % goat serum (Sigma) for 40 min at 37° C. The cells were then incubated with the anti-CD44 antibody (15 μg ml^{-1}) diluted in 2 % BSA in HBSS for 40 min at 37° C, followed by the Alexa-Fluor-647-conjugated goat anti-mouse secondary antibody (5 μg ml^{-1}) diluted in 2 % BSA in HBSS for 40 min at 37° C. The immunostained cells were fixed again in 3 % (w/v) paraformaldehyde and 0.2 % (w/v) glutaraldehyde in HBSS for 10 min at room temperature. The cells were then permeabilised in 0.1 % Triton X-100 (Sigma-Aldrich) in cytoskeleton buffer (10 mM MES (pH = 6.1), 150 mM NaCl, 5 mM EGTA, 5 mM glucose, and 5 mM $MgCl_2$) for 10 min at room temperature. The permeabilised cells were labelled for actin cytoskeleton with freshly prepared 0.5 μM Alexa-Fluor-488-conjugated phalloidin in the cytoskeleton buffer containing 1 % BSA for 1 hour at room temperature. Then, the cells were fixed again in 3 % (w/v) paraformaldehyde and 0.2 % (w/v) glutaraldehyde in HBSS for 10 min at room temperature. The cells were injected into poly-L-ornithine (Sigma)-coated microfluidic chambers (ibidi GmbH, sticky-slide VI 0.4) using the syringe pump and incubated overnight at 4° C.

The fluorescence imaging experiment of CD44 on the MβCD-treated fixed KG1a cells was conducted in a way similar to that on the fixed control KG1a cells by using a combination of the anti-CD44 antibody and the Alexa-Fluor-647-conjugated anti-mouse secondary antibody(AbuZineh et al., 2018). The cells were injected into poly-L-ornithine-coated microfluidic chambers (ibidi GmbH, sticky-slide VI 0.4) using the syringe pump and incubated overnight at 4° C.

For single-molecule tracking experiment of the PSGL-1 molecules on the control live KG1a cells (i.e. not rolling cells), the cells were blocked with Fc receptor blocker (Innovex Biosciences) for 45 min on ice, then the cells were immunostained by Alexa-Fluor-488-conjugated anti-PSGL-1 for 45 min on ice at much lower concentration (20 ng for each 10^6 cells) to sparsely label the PSGL-1 molecules localised on microvilli so that the motion of individual PSGL-1 molecules can be captured. The immunostained KG1a cells were suspended in HBSS at the density of 0.5 – 1×10^6 cells ml^{-1}. Then, the cells were injected into the microfluidic chambers (ibidi GmbH, glass-slide VI 0.5).

Fluorescence imaging. Fluorescence imaging experiments were conducted using a home-built wide-field fluorescence microscopy setup (Serag, Abadi, & Habuchi, 2014). Continuous wave (CW) solid-state laser operating at either 488nm (60 mW, Cobolt, MLD), 532 nm (100 mW, Cobolt, Samba), or 638 nm (60 mW, Cobolt, MLD) that passed an excitation filter (Semrock, LD01-640/8, FF01-532-12.5 or FF01-488/6 for the 638 nm, 532 nm or 488 nm excitation, respectively) and a beam expander (Thorlabs) was introduced into an inverted microscope (Olympus, IX71) through a focusing lane (f = 300 mm). The laser was reflected by a dichroic mirror (Semrock, FF660-Di02-25x36, Di01-R532-25x36, or FF506-Di03-25x36 for the 638 nm, 532 nm or 488 nm excitation, respectively) and the sample was illuminated through an objective

lens (Olympus, 100× NA = 1.49, UAPON 100XOTIRF, 60× NA = 1.3, UPLSAPO60XS2 or 40× NA = 1.25, UPLSAPO40XS). The excitation power was adjusted to 1 – 2 mW cm^{-2} at the sample plane using an acousto-optical tuneable filter (AOTF; AA Optoelectronics) inserted in the excitation beam pass. The fluorescence from the sample was captured by the same objective, separated from the illumination light by the same dichroic mirror, passed an emission bandpass filter (Semrock, FF01-697/58-25, FF01-580/60, or FF01-550/88 for the 638 nm, 532 nm or 488 nm excitation, respectively), and detected by an EMCCD camera (Andor Technology, iXon3 897). The fluorescence images were recorded with either 133-nm or 333-nm pixel size at 30 ms exposure time. The exposure of the EMCCD camera and the illumination of the sample by the excitation laser were synchronized by the AOTF using a laser control system (Andor Technology, PCUB-110). The image acquisition was done using the Andor iQ3 software. 3D fluorescence images were obtained by recording epi-fluorescence images of the cells at different Z-axis positions with 0.5 – 1.0 μm step size using a piezo objective scanner (PI PIFPC® P721) and reconstructing 3D images using ImageJ plugin.

Two-color fluorescence imaging experiments were conducted by introducing 638-nm and 488-nm lines of the lasers coaxially into the inverted microscope in the same way as the single-color excitation. The samples were excited through the objective lens (Olympus, 100× NA = 1.49, UAPON 100XOTIRF or 40× NA = 1.25, UPLSAPO40XS). The fluorescence from the sample was captured by the same objective, separated from the illumination light by a multiband dichroic mirror (Semrock, Di03-405/488/561/635-t1-25x36), and passed through a TuCam dual-camera adaptor (Andor Technology) equipped with a filter cassette containing a dichroic mirror (Semrock, FF580-FDi01-25x36) to separate the fluorescence into two channels. The separated

fluorescence from the samples was detected by two EMCCD cameras (Andor Technology, iXon3 897) through emission bandpass filters (Semrock, FF01-550/88-25 and FF01-697/58-25).

Determination of the number of PSGL-1 molecules on tethers and slings. The number of PSGL-1 molecules in each spot on the tethers and slings formed during KG1a cells rolling over E-selectin was calculated by comparing the integrated fluorescence intensity obtained from each PSGL-1 spot with the intensity obtained from single Alexa-Fluor-dye-conjugated anti-PSGL-1 antibody. To determine the fluorescence intensity obtained from single Alexa-Fluor-dye-conjugated anti-PSGL-1 antibody, the antibody was deposited on the surface of the microfluidic chamber at a concentration of 0.02 μg ml^{-1}. Fluorescence signals from the single deposited antibodies were captured at the experimental conditions identical to those for the imaging experiment on the immunostained KG1a cells rolling over E-selectin. We used only well-focused fluorescence images of the PSGL-1 spots on the tethers and slings for this analysis to ensure an accurate estimation of the number of the PSGL-1 molecules.

Single-molecule tracking analysis. Single-molecule tracking analysis of the PSGL-1 molecules moving along the tethers and slings of KG1a cells rolling over E-selectin and localised on the microvilli of control KG1a cells were conducted by generating single-molecule diffusion trajectories using a versatile tracking algorithm (Jaqaman et al., 2008; Serag & Habuchi, 2017). The algorithm uses a mixture-model fitting algorithm to localise and track multiple particles in the same field of view. It can detect the merging and splitting of particles during motion. To achieve these tracking targets, the algorithm localises and tracks all the local maxima in the single-molecule image including maxima that are partially overlapping along the tethers and slings. The diffusion rate (i.e. diffusion coefficient) and mode were analyzed by mean square

displacement (MSD) analysis (Kusumi, Sako, & Yamamoto, 1993). The MSD was calculated from the generated diffusion trajectories by using equation (1)

$$MSD(\Delta t) = \langle (x_{i+n} - x_i)^2 + (y_{i+n} - y_i)^2 \rangle, \quad (1)$$

where x_{i+n} and y_{i+n} demote the spatial positions after time interval Δt, given by the frame number, n, after starting at positions x_i and y_i. . The MSD-Δt profiles were fitted to random (equation (2)), and confined (equation (3)) diffusion models.

$$MSD(\Delta t) = 4D\Delta t, \quad (2)$$

where D is the diffusion coefficient,

$$MSD = \frac{L^2}{3}\left[1 - \exp\left(\frac{-12D\Delta t}{L^2}\right)\right], \quad (3)$$

where L is the side length of the confined area.

Super-resolution fluorescence imaging and analysis. Super-resolution (SR) fluorescence localisation microscopy imaging of fixed immunolabelled KG1a cells was performed in an imaging buffer composed of TN buffer (50 mM tris (pH 8.0) and 10 mM NaCl), oxygen scavenging system (glucose oxidase (0.5 mg ml^{-1}, Sigma), catalase (40 μg ml^{-1}, Sigma), 10% (w/v) glucose), and 100 mM β-mercaptoethanol (Sigma) as a reducing reagent. The imaging solution was prepared immediately before the imaging experiments. The imaging experiments were conducted on a custom-built wide-field illumination fluorescence microscope on an inverted optical microscope platform described above (Abadi, Serag, & Habuchi, 2018; AbuZineh et al., 2018). The fluorescence images were recorded using a 150 × 150 pixel region of the EMCCD camera with 83-nm pixel size at 10-ms exposure time. The fluorescence image

sequences with 10,000 frames were recorded for the reconstruction of SR localisation microscopy images.

The SR images were reconstructed by using either a custom-written MATLAB (MathWorks) code or Localizer software (Dedecker, Duwe, Neely, & Zhang, 2012). The positions of the AF-647 molecules were determined by 2D Gaussian fitting of the images. We removed fluorescence spots whose width was significantly larger (>200 nm) than the point spread function (PSF) of the optical system (PSF, ~130 nm) from the analysis. The effect of the stage drift in the *xy* plane was corrected by reconstructing the subimages using 5000 localisations. In the two-colour SR imaging, TetraSpeck microspheres (diameter, 100 nm) deposited on a cleaned coverslip was used to calibrate the shift between the two channels. Using fluorescence images of the TetraSpeck microspheres recorded simultaneously on the two cameras, we generated a registration map that corrects the shift between the two images and applied the registration map to the images obtained from the cell samples.

Scanning electron microscopy. The harvested KG1a cells (10^7 cells) were washed twice with HBSS. The cells were fixed in 2-2.5% glutaraldehyde in 0.1 M Cacodylate buffer (pH = 7.2 – 7.4) in 4°C for overnight. The fixed cells were washed three times with the 0.1 M Cacodylate buffer with 15 min submerged in buffer before the next wash and resuspended in the 200 µl of the buffer. Then, 100 µl of the cell suspension was added on a cover slip, which was brushed with polylysine and incubated overnight inside a moisturized chamber before use. The cells were further fixed in 1% osmium tetroxide in 0.1 M Cacodylate buffer for one hour in dark. The cells were washed three times with distilled water, where they were submerged in water for 15 min before the next wash, and dehydrated in gradient ethanol (30, 50, 70, 90 and 100 %). Samples were carried further onto Critical Point Drying apparatus and covered with 100 % ethanol to

completely submerge the samples. The dehydrated cells were placed on a holder of the scanning electron microscope (SEM) and coated with 4mm platinum (K575X Sputter Coater, Quorum). The SEM images were recorded using Teneo SEM (Thermo Fischer).

Flow cytometry. Binding specificity of the mouse anti-human PSGL-1 and mouse anti-human CD44 antibodies, which were used for the fluorescence imaging experiments, to PSGL-1 and CD44 on KG1a cells were evaluated by flow cytometry. KG1a cells (10^6 cells ml^{-1}) were incubated with either anti-human PSGL-1 antibody (clone KPL-1, Ms IgG1, κ), anti-human CD44 antibody (clone 515 Ms IgG1, κ, or 2C5 Ms IgG2a) or purified mouse IgG1κ isotype (BioLegend) at a final concentration of 10 μg ml^{-1} in HBSS at 4°C for 30 min. Subsequently, the KG1a cells were incubated with Alexa-Fluor-488–conjugated goat anti-mouse antibody (5 μg ml^{-1}, IgG, Invitrogen) in HBSS at 4°C for 20 min. For the secondary antibody control, KG1a cells (10^6 cells ml^{-1}) were incubated with Alexa-Fluor-488–conjugated goat anti-mouse antibody (5 μg ml^{-1}) in HBSS at 4°C for 20 min. The fluorescence intensity was determined using a FACSCanto flow cytometer (Beckman Dickenson).

Western Blot Analysis. WT KG1a, scrambled, or CD34 siRNA knockdown cells were lysed using a cell lysis buffer containing 88% NP40 (Invitrogen™ Novex™, Fisher Scientific), 10% protease inhibitor (Pierce™, Thermo Scientific), 1% PMSF, and 1% Phosphatase inhibitor (Halt™, Thermo Scientific) at 4°C for 1 h. The whole cell lysate was collected and incubated with NuPAGE LDS sample buffer (Invitrogen) and 10% β-mercaptoethanol at 70°C for 10 min. The samples were then run on an SDS-PAGE gel prior to being transferred to a PVDF membrane. The PVDF membrane was blocked overnight at 4°C using Tris-buffered saline with Tween-20 (Cell Signaling Technology) containing 5% non-fat skim milk powder. The membrane was then washed and incubated with a mouse anti-human CD34 antibody (QBEND/10, BIO

RAD). The membrane was then washed and immunoblotted with HRP-conjugated secondary antibodies prior to imaging.

ACKNOWLEDGMENT

We thank Ms. Ohoud M. Alharbi for the SEM images of KG1a cells. The research reported in this publication was supported by funding from the King Abdullah University of Science and Technology (KAUST) and the KAUST Office of Sponsored Research under Award No. CRG R2 13 MERZ KAUST 1. We would like to thank Ms. Samar A. Rustum and Ms. Umm Habiba for their support in the management of the lab.

ADDITIONAL INFORMATION

AUTHOR CONTRIBUTIONS

S.H. and J.S.M conceived the project. B.A.A. designed the in vitro cell rolling assay and single-molecule fluorescence imaging experiments. K.A.Z. designed the super-resolution fluorescence microscopy experiments. A.R. prepared cells for SEM imaging? B.A.A. and A.R. conducted the fluorescence imaging experiments with the support of S.N. and analysed the data with the support of M.F.S. K.A.Z. conducted the super-resolution fluorescence imaging experiments and analyzed the data. B.A.A. conducted the flow cytometry experiments with the support of F.A. M.A. prepared the CD34 knockdown KG1a cells. A.S.A. prepared the primary $CD34^{pos}$-HSPCs. M.A., A.S.A., A.R., and S.N. conducted and analysed the fluorescence imaging experiments related to the CD34 knockdown KG1a cells and the primary human $CD34^{pos}$-HSPCs. J.S.M. provided the cell lines. S.H., J.S.M., and B.A.A. wrote the manuscript. All authors discussed the results.

COMPETING INTERESTS

The authors declare no competing interests.

Supplementary information is available for this paper.

REFERENCES

Abadi, M., Serag, M. F., & Habuchi, S. (2018). Entangled polymer dynamics beyond reptation. *Nature Communications, 9*, 5098. doi:10.1038/s41467-018-07546-7

Abbal, C., Lambelet, M., Bertaggia, D., Gerbex, C., Martinez, M., Arcaro, A., . . . Spertini, O. (2006). Lipid raft adhesion receptors and Syk regulate selectin-dependent rolling under flow conditions. *Blood, 108*(10), 3352-3359. doi:10.1182/blood-2006-04-013912

AbuSamra, D. B., Al-Kilani, A., Hamdan, S. M., Sakashita, K., Gadhoum, S. Z., & Merzaban, J. S. (2015). Quantitative characterization of E-selectin interaction with native CD44 and P-selectin glycoprotein ligand-1 (PSGL-1) using a real time immunoprecipitation-based binding assay. *Journal of Biological Chemistry, 290*(35), 21213-21230. doi:10.1074/jbc.M114.629451

AbuSamra, D. B., Aleisa, F. A., Al-Amoodi, A. S., Jalal Ahmed, H. M., Chin, C. J., Abuelela, A. F., . . . Merzaban, J. S. (2017). Not just a marker: CD34 on human hematopoietic stem/progenitor cells dominates vascular selectin binding along with CD44. *Blood Adv, 1*(27), 2799-2816. doi:10.1182/bloodadvances.2017004317

AbuZineh, K., Joudeh, L. I., Al Alwan, B., Hamdan, S. M., Merzaban, J. S., & Habuchi, S. (2018). Microfluidics-based super-resolution microscopy enables nanoscopic characterization of blood stem cell rolling. *Science Advances, 4*(7), eaat5304. doi:10.1126/sciadv.aat5304

Alon, R., Hammer, D. A., & Springer, T. A. (1995). Lifetime of the P-selectin-carbohydrate bond and its response to tensile force in hydrodynamic flow. *Nature, 374*(6522), 539-542. doi:10.1038/374539a0

Chen, S. Q., & Springer, T. A. (1999). An automatic braking system that stabilizes leukocyte rolling by an increase in selectin bond number with shear. *Journal of Cell Biology, 144*(1), 185-200. doi:10.1083/jcb.144.1.185

Cummings, R. D., & McEver, R. P. (2009). C-type lectins. In A. Varki, R. D. Cummings, J. D. Esko, H. H. Freeze, P. Stanley, C. R. Bertozzi, G. W. Hart, & M. E. Etzler (Eds.), *Essentials of glycobiology*. Cold Spring Harbor (NY): Cold Spring Harbor Laboratory Press.

Dedecker, P., Duwe, S., Neely, R. K., & Zhang, J. (2012). Localizer: fast, accurate, open-source, and modular software package for superresolution microscopy. *Journal of Biomedical Optics, 17*(12), 5. doi:10.1117/1.jbo.17.12.126008

Dimitroff, C. J., Lee, J. Y., Rafii, S., Fuhlbrigge, R. C., & Sackstein, R. (2001). CD44 is a major E-selectin ligand on human hematopoietic progenitor cells. *Journal of Cell Biology, 153*(6), 1277-1286. doi:10.1083/jcb.153.6.1277

Evans, E., Heinrich, V., Leung, A., & Kinoshita, K. (2005). Nano- to microscale dynamics of P-selectin detachment from leukocyte interfaces. I. Membrane separation from the cytoskeleton. *Biophysical Journal, 88*(3), 2288-2298. doi:10.1529/biophysj.104.051698

Frenette, P. S., Subbarao, S., Mazo, I. B., von Andrian, U. H., & Wagner, D. D. (1998). Endothelial selectins and vascular cell adhesion molecule-1 promote hematopoietic progenitor homing to bone marrow. *Proceedings of the National Academy of Sciences of the United States of America, 95*(24), 14423-14428. doi:10.1073/pnas.95.24.14423

Gaborski, T. R., Clark, A., Waugh, R. E., & McGrath, J. L. (2008). Membrane Mobility of beta 2 Integrins and Rolling Associated Adhesion Molecules in Resting Neutrophils. *Biophysical Journal, 95*(10), 4934-4947. doi:10.1529/biophysj.108.132886

Goetz, D. J., Greif, D. M., Ding, H., Camphausen, R. T., Howes, S., Comess, K. M., . . . Luscinskas, F. W. (1997). Isolated P-selectin glycoprotein ligand-1 dynamic adhesion to P- and E-selectin. *Journal of Cell Biology, 137*(2), 509-519. doi:10.1083/jcb.137.2.509

Heinrich, V., Leung, A., & Evans, E. (2005). Nano- to microscale dynamics of P-selectin detachment from leukocyte interfaces. II. Tether flow terminated by P-selectin dissociation from PSGL-1. *Biophysical Journal, 88*(3), 2299-2308. doi:10.1529/biophysj.104.051706

Hidalgo, A., Weiss, L. A., & Frenette, P. S. (2002). Functional selectin ligands mediating human CD34(+) cell interactions with bone marrow endothelium are enhanced postnatally. *Journal of Clinical Investigation, 110*(4), 559-569. doi:10.1172/jci200214047

Jaqaman, K., Loerke, D., Mettlen, M., Kuwata, H., Grinstein, S., Schmid, S. L., & Danuser, G. (2008). Robust single-particle tracking in live-cell time-lapse sequences. *Nature Methods, 5*(8), 695-702. doi:10.1038/nmeth.1237

Kolaczkowska, E., & Kubes, P. (2013). Neutrophil recruitment and function in health and inflammation. *Nature Reviews Immunology, 13*(3), 159-175. doi:10.1038/nri3399

Kusumi, A., Sako, Y., & Yamamoto, M. (1993). Confined lateral diffusion of membrane receptors as studied by single particle tracking (nanovid microscopy). Effects of calcium-induced differentiation in cultured epithelial cells. *Biophys J, 65*(5), 2021-2040. doi:10.1016/S0006-3495(93)81253-0

Lehr, J. E., & Pienta, K. J. (1998). Preferential adhesion of prostate cancer cells to a human bone marrow endothelial cell line. *Journal of the National Cancer Institute, 90*(2), 118-123. doi:10.1093/jnci/90.2.118

Ley, K., Hoffman, H. M., Kubes, P., Cassatella, M. A., Zychlinsky, A., Hedrick, C. C., & Catz, S. D. (2018). Neutrophils: New insights and open questions. *Science Immunology, 3*(30), 14. doi:10.1126/sciimmunol.aat4579

Ley, K., Laudanna, C., Cybulsky, M. I., & Nourshargh, S. (2007). Getting to the site of inflammation: the leukocyte adhesion cascade updated. *Nature Reviews Immunology, 7*(9), 678-689. doi:10.1038/nri2156

Lukinavicius, G., Reymond, L., D'Este, E., Masharina, A., Gutfert, F., Ta, H., . . . Johnsson, K. (2014). Fluorogenic probes for live-cell imaging of the cytoskeleton. *Nature Methods, 11*(7), 731-U168. doi:10.1038/nmeth.2972

Magnon, C., & Frenette, P. S. (2008). Hematopoietic stem cell trafficking. In *StemBook*.

Marki, A., Gutierrez, E., Mikulski, Z., Groisman, A., & Ley, K. (2016). Microfluidics-based side view flow chamber reveals tether-to-sling transition in rolling neutrophils. *Scientific Reports, 6*, 8. doi:10.1038/srep28870

Marshall, B. T., Long, M., Piper, J. W., Yago, T., McEver, R. P., & Zhu, C. (2003). Direct observation of catch bonds involving cell-adhesion molecules. *Nature, 423*(6936), 190-193. doi:10.1038/nature01605

Mazo, I. B., Gutierrez-Ramos, J. C., Frenette, P. S., Hynes, R. O., Wagner, D. D., & von Andrian, U. H. (1998). Hematopoietic progenitor cell rolling in bone marrow microvessels: Parallel contributions by endothelial selectins and vascular cell adhesion molecule 1. *Journal of Experimental Medicine, 188*(3), 465-474. doi:10.1084/jem.188.3.465

McEver, R. P., & Zhu, C. (2010). Rolling cell adhesion. *Annual Review of Cell and Developmental Biology, 26*, 363-396. doi:10.1146/annurev.cellbio.042308.113238

Merzaban, J. S., Burdick, M. M., Gadhoum, S. Z., Dagia, N. M., Chu, J. T., Fuhlbrigge, R. C., & Sackstein, R. (2011). Analysis of glycoprotein E-selectin ligands on human and mouse marrow cells enriched for hematopoietic stem/progenitor cells. *Blood, 118*(7), 1774-1783. doi:10.1182/blood-2010-11-320705

Miner, J. J., Xia, L., Yago, T., Kappelmayer, J., Liu, Z., Klopocki, A. G., . . . McEver, R. P. (2008). Separable requirements for cytoplasmic domain of PSGL-1 in leukocyte rolling and signaling under flow. *Blood, 112*(5), 2035-2045. doi:10.1182/blood-2008-04-149468

Moore, K. L., Patel, K. D., Bruehl, R. E., Li, F. G., Johnson, D. A., Lichenstein, H. S., . . . McEver, R. P. (1995). P-selectin glycoprotein ligand-1 mediates rolling of human neutrophils on P-selectin. *Journal of Cell Biology, 128*(4), 661-671. doi:10.1083/jcb.128.4.661

Ponta, H., Sherman, L., & Herrlich, P. A. (2003). CD44: From adhesion molecules to signalling regulators. *Nature Reviews Molecular Cell Biology, 4*(1), 33-45. doi:10.1038/nrm1004

Quail, D. F., & Joyce, J. A. (2013). Microenvironmental regulation of tumor progression and metastasis. *Nature Medicine, 19*(11), 1423-1437. doi:10.1038/nm.3394

Schmidtke, D. W., & Diamond, S. L. (2000). Direct observation of membrane tethers formed during neutrophil attachment to platelets or P-selectin under physiological flow. *Journal of Cell Biology, 149*(3), 719-729. doi:10.1083/jcb.149.3.719

Schweitzer, K. M., Drager, A. M., vanderValk, P., Thijsen, S. F. T., Zevenbergen, A., Theijsmeijer, A. P., . . . Langenhuijsen, M. (1996). Constitutive expression of E-selectin and vascular cell adhesion molecule-1 on endothelial cells of hematopoietic tissues. *American Journal of Pathology, 148*(1), 165-175. Retrieved from <Go to ISI>://WOS:A1996TP29100018

Serag, M. F., Abadi, M., & Habuchi, S. (2014). Single-molecule diffusion and conformational dynamics by spatial integration of temporal fluctuations. *Nature Communications, 5*, 10. doi:10.1038/ncomms6123

Serag, M. F., & Habuchi, S. (2017). Conserved linear dynamics of single-molecule Brownian motion. *Nature Communications, 8*, 15675.

Setiadi, H., & McEver, R. P. (2008). Clustering endothelial E-selectin in clathrin-coated pits and lipid rafts enhances leukocyte adhesion under flow. *Blood, 111*(4), 1989-1998. doi:10.1182/blood-2007-09-113423

Shao, J. Y., Ting-Beall, H. P., & Hochmuth, R. M. (1998). Static and dynamic lengths of neutrophil microvilli. *Proceedings of the National Academy of Sciences of the United States of America, 95*(12), 6797-6802. doi:10.1073/pnas.95.12.6797

Snapp, K. R., Heitzig, C. E., & Kansas, G. S. (2002). Attachment of the PSGL-1 cytoplasmic domain to the actin cytoskeleton is essential for leukocyte rolling on P-selectin. *Blood, 99*(12), 4494-4502. doi:10.1182/blood.V99.12.4494

Sundd, P., Gutierrez, E., Koltsova, E. K., Kuwano, Y., Fukuda, S., Pospieszalska, M. K., . . . Ley, K. (2012). 'Slings' enable neutrophil rolling at high shear. *Nature, 488*(7411), 399-403. doi:10.1038/nature11248

Sundd, P., Pospieszalska, M. K., & Ley, K. (2013). Neutrophil rolling at high shear: Flattening, catch bond behavior, tethers and slings. *Molecular Immunology, 55*(1), 59-69. doi:10.1016/j.molimm.2012.10.025

Wang, Y., Yago, T., Zhang, N., Abdisalaam, S., Alexandrakis, G., Rodgers, W., & McEver, R. P. (2014). Cytoskeletal Regulation of CD44 Membrane Organization and Interactions with E-selectin. *Journal of Biological Chemistry, 289*(51), 35159-35171. doi:10.1074/jbc.M114.600767

Yago, T., Fu, J. X., McDaniel, J. M., Miner, J. J., McEver, R. P., & Xia, L. J. (2010). Core 1-derived O-glycans are essential E-selectin ligands on neutrophils. *Proceedings of the National Academy of Sciences of the United States of America, 107*(20), 9204-9209. doi:10.1073/pnas.1003110107

FIGURES AND LEGENDS

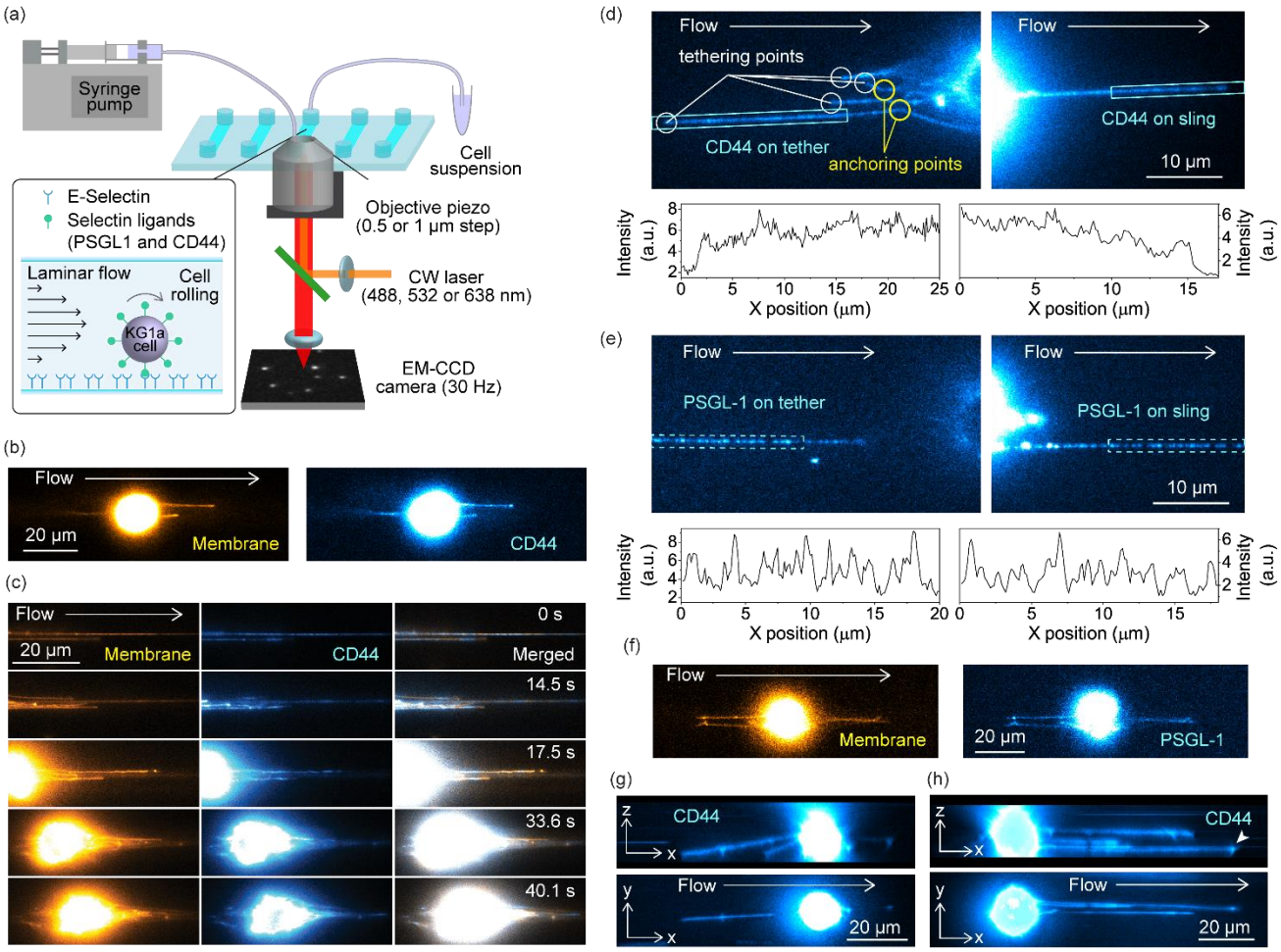

Figure 1. Single-molecule visualization of selectin ligands on the tethers and slings. (a) Schematic illustration describing the custom-built microfluidics-based single-molecule imaging setup. Continuous-wave lasers were introduced into an inverted optical microscope through a focusing lens, resulting in a wide-field illumination of the samples through the objectives (40x, NA 1.25, silicone immersion, or 100x, NA 1.49, oil immersion). Fluorescently-labelled or stained KG1a cells were injected to a microfluidic chamber whose surface was coated by rh E-selectin molecules (15 molecules μm^{-2}). The shear stress was set to 1 – 8 dyne cm^{-2}. The fluorescence images were recorded by an EM-CCD camera at a frame rate of 33 Hz. The axial position of the microscope stage was controlled by an objective piezo scanner. (b) Two-color fluorescence images of the cell membrane (stained by Vybrant DiO dye) and CD44 (immunostained by Alexa-Fluor-647-conjugated anti-CD44 antibody, clone 515) captured during the KG1a cell rolling over the surface-deposited E-selectin molecules. The stained and labelled cells were injected into the microfluidic chambers whose surface was coated by the rh E-selectin molecules with the density of 15 molecules μm^{-2}. The cells were injected into the chambers at a shear stress of 2 dyne cm^{-2}. (c) Time-lapse two-colour fluorescence images of the cell membrane (stained by Vybrant DiO dye) and CD44 (immunostained by Alexa-Fluor-647-conjugated anti-

CD44 antibody, clone 515) captured during the cells rolling over the surface-deposited E-selectin molecules. The merged images are displayed in the right panels. The stained and labelled cells were injected into the microfluidic chambers whose surface was coated by the rh E-selectin molecules with the density of 15 molecules μm^{-2}. The cells were injected into the chambers at a shear stress of 2 dyne cm^{-2}. (d) Immunofluorescence image of the CD44 molecules on the tethers (top left) and slings (top right) formed during cell rolling over E-selectin (15 molecules μm^{-2}) at a shear stress of 2 dyne cm^{-2}. The bottom left and bottom right panels show fluorescence intensity profiles along the tethers and slings obtained from cyan regions in the top left and top right panels, respectively. (e) Fluorescence image of the PSGL-1 molecules (immunostained by Alexa-Fluor-555-conjugated anti-PSGL-1 antibody, clone KPL-1) on the tethers (top left) and slings (top right) formed during cell rolling over E-selectin (15 molecules μm^{-2}) at a shear stress of 2 dyne cm^{-2}. The bottom left and bottom right panels show fluorescence intensity profiles along the tethers and slings obtained from cyan regions in the top left and top right panels, respectively. (f) Two-colour fluorescence images of the cell membrane (stained by Vybrant DiO dye) and PSGL-1 (immunostained by Alexa-Fluor-647-conjugated anti-PSGL-1 antibody, clone KPL-1) captured during the KG1a cell rolling over the surface-deposited E-selectin molecules (15 molecules μm^{-2}) at a shear stress of 2 dyne cm^{-2}. Side views (top) and top views (bottom) of the 3D reconstructed fluorescence images of the CD44 molecules (immunostained by Alexa-Fluor-488-conjugated anti-CD44 antibody, clone 515) on the (g) tethers and (h) slings captured during the cells rolling over E-selectin (15 molecules μm^{-2}) at a shear stress of 2 dyne cm^{-2}. The 3D images were reconstructed by recording fluorescence images of the cell at (g) 57 and (h) 59 different Z-axis positions with 0.5 μm step size.

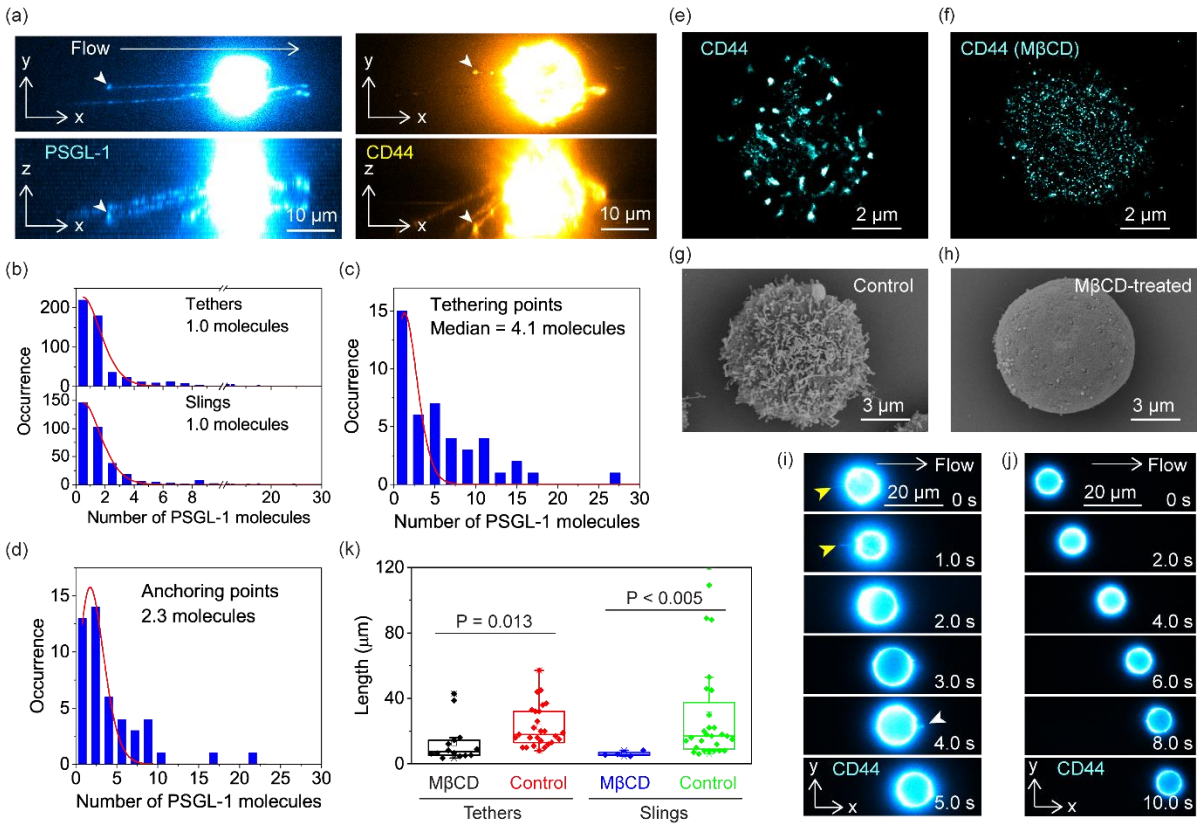

Figure 2. Spatial clustering of the selectin ligands on microvilli enables efficient formation of tethers and slings. (a) Top views (top) and side views (bottom) of the 3D reconstructed fluorescence images of the PSGL-1 molecules (left, immunostained by Alexa-Fluor-555-conjugated anti-PSGL-1 antibody clone KPL-1) and CD44 molecules (right, immunostained by Alexa-Fluor-647-conjugated anti-CD44 antibody, clone 515) captured during the KG1a cells rolling over E-selectin (15 molecules μm^{-2}) at a shear stress of 2 dyne cm^{-2}. The 3D images were reconstructed by recording fluorescence images of the cell at 40 different Z-axis positions with 1 μm step size (PSGL-1) or 59 different Z-axis positions with 0.5 μm step size (CD44). Frequency histograms of the number of the PSGL-1 molecules in each spot on the (b) tethers (top) and slings (bottom) and at the (c) tethering points and (d) anchoring points of the KG1a cells. The solid lines show Poissonian fittings. Super-resolution fluorescence localisation microscopy images of CD44 (immunostained by anti-CD44 515 antibody followed by Alexa-Fluor-647-conjugated secondary antibodies) on the (e) control and (f) methyl-β-cyclodextrin (MβCD)-treated KG1a cells. Scanning electron microscopy images of (g) control and (h) MβCD-treated KG1a cells. (i) Time-lapse fluorescence images of the CD44 molecules (immunostained by Alexa-Fluor-647-conjugated anti-CD44 antibody, clone 515) captured during the MβCD-treated KG1a cell rolling over E-selectin (15 molecules μm^{-2}) at a shear stress of 2 dyne cm^{-2}. The yellow and white arrowheads highlight tether and sling, respectively. (j) Time-lapse fluorescence images of the CD44 molecules (immunostained by Alexa-Fluor-647-conjugated anti-CD44 antibody clone 515) captured during CD34 knockdown (CD34-KD) KG1a cell rolling over E-selectin (15 molecules μm^{-2}) at a shear stress of 2 dyne cm^{-2}. (k) Box plots showing the length of individual tethers and slings on the control and MβCD-treated KG1a cells. The cells were

injected into the microfluidic chambers whose surface was coated with rh E-selectin molecules at a density of 15 molecules μm^{-2}. The cells were injected into the chambers at a shear stress of 2 dyne cm^{-2}.

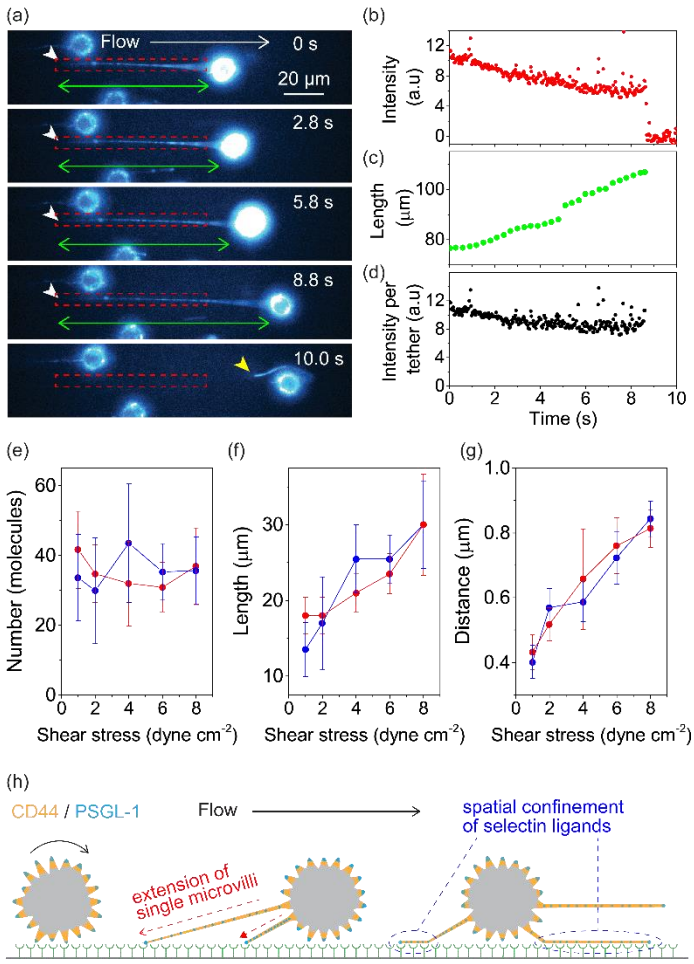

Figure 3. Spatial confinement of the selectin ligands to the tethers and slings. (a) Time-lapse fluorescence images of the PSGL-1 molecules (immunostained by Alexa-Fluor-555-conjugated anti-PSGL-1 antibody, clone KPL-1) on the KG1a cell captured during cell rolling over E-selectin (15 molecules μm^{-2}) at a shear stress of 2 dyne cm^{-2}, which shows the elongation of the tether. The white arrowheads show the tethering point. The yellow arrowhead show the tether detached from the surface E-selectin. (b) Time-lapse integrated fluorescence intensities of the PSGL-1 molecules obtained from the region designated by the red dashed boxes in (a). (c) Time-dependent change in the length of the tether obtained from the time-lapse fluorescence images of PSGL-1 displayed in (a) green arrows. (d) Time-dependent change in the integrated fluorescence intensity of the PSGL-1 molecules obtained from the whole tether formed during cell rolling displayed in (a). Shear stress dependence of the (e) mean numbers of the PSGL-1 molecules per tether and sling, (f) mean lengths of the tether and sling, and (g) mean distances between adjacent PSGL-1 molecules on the tether and sling. The error bars show the standard deviations determined by 19 – 58 data. (h) Schematic illustration describing how the spatial confinement of the selectin ligands into the tethers and slings due to the formation of individual tethers from single microvilli promote stable and slow rolling of the cell on E-selectin.

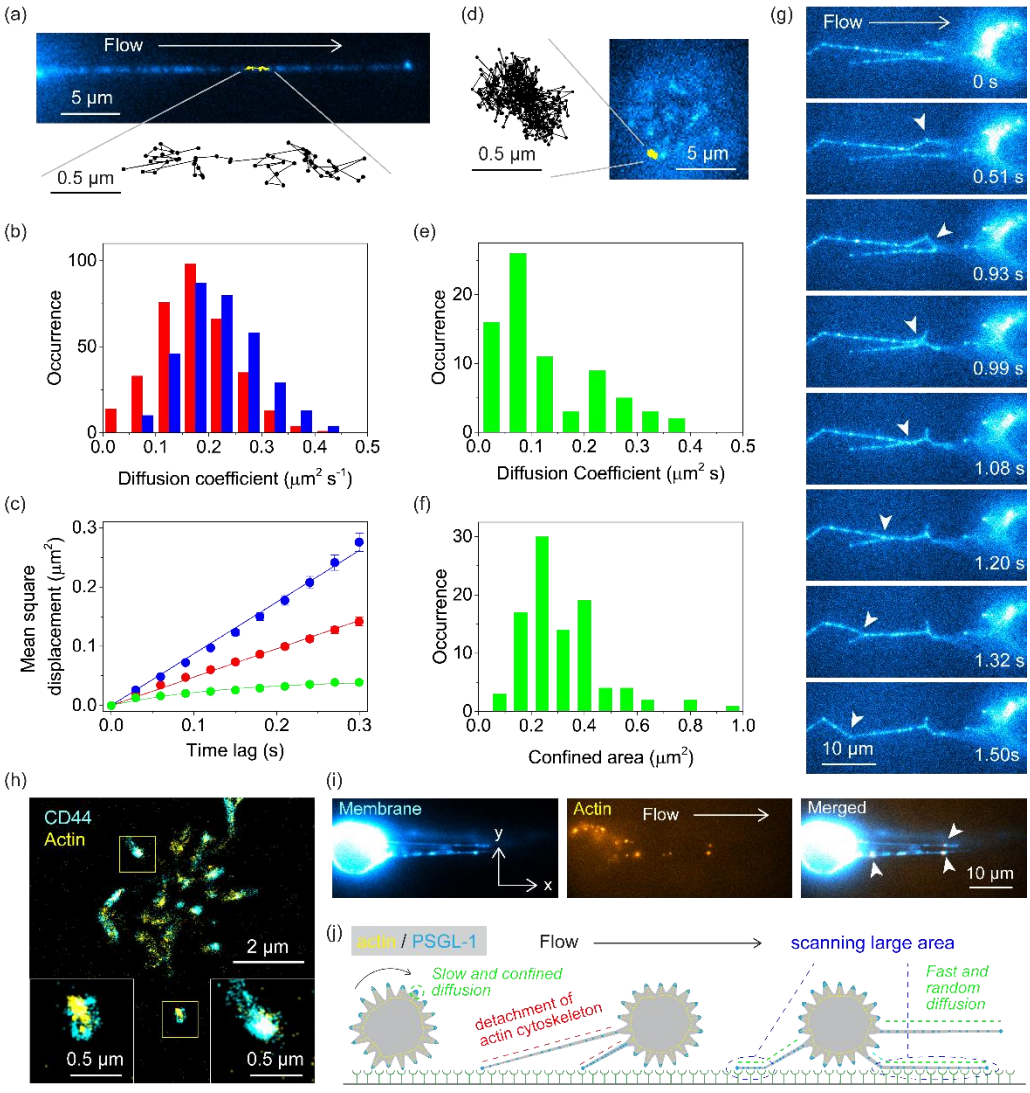

Figure 4. Detachment of cell membrane from actin cytoskeleton during the tether formation promotes efficient selectin-ligands binding. (a) Single-molecule fluorescence images of PSGL-1 (immunostained by Alexa-Fluor-555-conjugated anti-PSGL-1 antibody, clone KPL-1) on the sling of the KG1a cell formed during cell rolling over E-selectin (15 molecules μm^{-2}) at a shear stress of 2 dyne cm^{-2}. An example of the single-molecule diffusion trajectories obtained from the time-lapse fluorescence images is shown by the yellow line. (b) Frequency histograms of the diffusion coefficient of the PSGL-1 molecules on the tethers (red) and slings (blue) of the KG1a cells formed during cell rolling over E-selectin (15 molecules μm^{-2}) at a shear stress of 2 dyne cm^{-2}. The diffusion coefficients were calculated by fitting the mean square displacement (MSD) plots obtained from the individual diffusion trajectories to Eq. 2. (c) MSD versus time lag plots obtained for the PSGL-1 molecules on the tethers (red), slings (blue), and microvilli of the KG1a cells. The error bars show the standard errors of the mean determined by 340, 328, and 129 MSD plots for the tether, sling, and microvilli, respectively. (d) Single-molecule fluorescence images of PSGL-1 (immunostained by Alexa-Fluor-488-conjugated anti-PSGL-1 antibody, clone KPL-1) on the microvilli of the control KG1a cell. An example of the

single-molecule diffusion trajectories obtained from the time-lapse fluorescence images is shown in the yellow line. (e) Frequency histograms of the diffusion coefficient of the PSGL-1 molecules on the microvilli of the control KG1a cells. The diffusion coefficients were calculated by fitting the MSD plots obtained from the individual diffusion trajectories to Eq. 3. (f) Frequency histogram of the confine area of the diffusing PSGL-1 molecules on the microvilli of the control KG1a cells. The confined areas were calculated by fitting the MSD plots obtained from the individual diffusion trajectories to Eq. 3. (g) Time-lapse fluorescence images of the PSGL-1 molecule (immunostained by Alexa-Fluor-555-conjugated anti-PSGL-1 antibody, clone KPL-1) on the KG1a cell captured during cell rolling over E-selectin (15 molecules μm^{-2}) at a shear stress of 2 dyne cm^{-2}, which show the merger of the multiple tethers. The white arrowheads show the regions in which the merger of the tethers occurs. (h) Two-colour super-resolution fluorescence localisation microscopy image of CD44 (cyan, immunostained by anti-CD44 515 antibody followed by Alexa-Fluor-647-conjugated secondary antibodies) and actin (yellow, labelled by Alexa-Fluor-488-conjugated phalloidin) on the control KG1a cell. The insets show enlarged views of the yellow regions. (i) Two-colour fluorescence images of the cell membrane (cyan, stained by Vybrant DiO dye) and actin (yellow, labelled by silicon-rhodamine-conjugated jasplakinolide) on the slings of the KG1a cells formed during cell rolling over E-selectin (15 molecules μm^{-2}) at a shear stress of 2 dyne cm^{-2}. The white arrowheads show the regions in which the patches of actin colocalise with the slings. (j) Schematic illustration describing how the faster and random diffusional motion of the selectin ligands on the tethers and slings, due to the detachment of the cell membrane from the cortical actin cytoskeleton during the tether formation, promote stable and slow rolling the cell on E-selectin.